Organic Geochemistry 150 (2020) 104120

Contents lists available at ScienceDirect

Organic Geochemistry

journal homepage: www.elsevier.com/locate/orggeochem

Plant wax evidence for precipitation and vegetation change from a coastal sinkhole lake in the Bahamas spanning the last 3000 years

Anne E. Tamalavage [a,g,*,1], Peter J. van Hengstum [a,b], Patrick Louchouarn [a,b], Patricia L. Fall [c], Jeffrey P. Donnelly [d], Nancy A. Albury [e], Sloan Coats [f], Sarah J. Feakins [g,*]

[a] Department of Oceanography, Texas A&M University, College Station, TX, USA
[b] Department of Marine Science, Texas A&M University at Galveston, Galveston, TX, USA
[c] Department of Geography and Earth Sciences, University of North Carolina Charlotte, Charlotte, NC 28223, USA
[d] Department of Geology and Geophysics, Woods Hole Oceanographic Institution, Woods Hole, MA, USA
[e] Antiquities, Monuments, and Museums Corporation/National Museum of the Bahamas, Nassau, Bahamas
[f] Department of Earth Sciences, University of Hawai'i at Manoa, Honolulu, HI, USA
[g] Department of Earth Sciences, University of Southern California, Los Angeles, CA, USA

ARTICLE INFO

Article history:
Received 8 March 2020
Received in revised form 30 June 2020
Accepted 4 September 2020
Available online 8 September 2020

Keywords:
Plant wax
Hydrogen isotopes
Carbon isotopes
Coastal Sinkhole
Holocene
Caribbean
Bahamas
Hydroclimate

ABSTRACT

Plant wax hydrogen isotopic composition is commonly used to reconstruct the hydrogen isotopic composition of precipitation used by terrestrial vegetation. However, mangroves growing in coastal environments take up a mixture of freshwater and seawater. Biosynthetic fractionation (between source water and plant wax) differs between plant types and as a function of salinity, potentially complicating interpretations of past precipitation in coastal environments. In order to reconstruct Holocene hydrologic and ecologic changes archived within sediments from Blackwood Sinkhole on Abaco Island in The Bahamas, we adopt a multi-proxy approach using plant wax hydrogen isotopic composition (δ^2H) to reconstruct paleohydrology, together with plant wax carbon isotopic composition ($\delta^{13}C_{wax}$), sterol biomarkers and pollen abundances to identify vegetation change. When pollen indicates a stable terrestrial plant community (2950–850 cal yrs BP), variations of δ^2H values measured on the plant wax C_{28} *n*-alkanoic acid are interpreted in terms of precipitation isotope (δ^2H_{precip}) changes, with ^2H-depletion from 2950 to ~2100 cal yrs BP and ~1700 to 1000 cal yrs BP. However, interpretation is complicated at 850 cal yrs BP, when δ^2H values decrease (−50‰) concurrent with increased *Laguncularia racemosa* (white mangrove) and *Conocarpus erectus* (buttonwood mangrove), and the mangrove-derived biomarker, taraxerol. We develop a pollen-based correction for mangrove inputs, yielding reconstructed precipitation isotope estimates ($\delta^2H_{precip\text{-}corr}$). Low $\delta^2H_{precip\text{-}corr}$ values are synchronous with increased abundance of pine pollen, both of which may indicate wetter conditions from 850 cal yrs BP to present. This study provides additional evidence that mangroves can complicate hydrologic reconstructions from *n*-alkyl terrestrial plant wax biomarkers, and that such complication can be removed by pollen-based correction. After correcting for mangrove inputs, we obtain estimates of $\delta^2H_{precip\text{-}corr}$ from −33 to +25‰ throughout the last 2950 years, with uncertainties on the order of 10–20‰.

1. Introduction

Many small island nations in the Caribbean with limited water storage capacity are at risk of extreme freshwater stress in the 21st century (Lin et al., 2015; Karnauskas et al., 2016; Karnauskas et al., 2018). The Caribbean region has been susceptible to drought throughout the historical and satellite intervals, including a severe drought in 2013–2016 (Herrera et al., 2018). Although there is evidence for an overall drying pattern from the middle Holocene to the present associated with Holocene insolation patterns (Hodell et al., 1991), there also have been multiple severe droughts on centennial timescales (Horn and Sanford Jr, 1992; Lane et al., 2009; Fritz et al., 2011; Malaizé et al., 2011). Such variations in regional climate have been proposed to cause ecological change in The Bahamas (Kjellmark, 1996; Slayton, 2010), and have been linked

* Corresponding authors at: Department of Oceanography, Texas A&M University, College Station, TX, USA; Department of Earth Sciences, University of Southern California, Los Angeles, CA, USA.
E-mail addresses: atamalavage91@tamu.edu (A.E. Tamalavage), feakins@usc.edu (S.J. Feakins).
[1] Present address: Department of Marine Science, Texas A&M University at Galveston, TX, USA.

https://doi.org/10.1016/j.orggeochem.2020.104120
0146-6380/

to socioeconomic transitions among the Mayans in the Yucatan (Hodell et al., 1991; Haug et al., 2003) and smaller populations in the Dominican Republic (Lane et al., 2014). Yet, there may be opposing signs of hydroclimate change across the Caribbean (Bhattacharya and Coats, 2020). Additional drought records are needed, and here we test plant waxes for their potential to reconstruct hydroclimate in the Caribbean.

Plant wax hydrogen isotopic applications in tropical and subtropical climates include evidence for changes in Holocene hydroclimate in India based on *n*-alkanes (Sarkar et al., 2015), and changes in *n*-alkanoic acids across the last glacial period into the Holocene driven by the South American Southern Monsoon (Fornace et al., 2014) and the North American Monsoon (Bhattacharya et al., 2017). Central American and Caribbean plant wax *n*-alkane records include those from the highlands of Costa Rica (Lane and Horn, 2013), and lakes in the lesser Antilles (Lane et al., 2014). However, there are a limited number of plant wax reconstructions derived from sinkhole or blue hole basins, including sinkhole sedimentary records studied in the Yucatan (Douglas et al., 2012).

In general, the hydrogen isotopic composition of biomarkers is correlated to source water modified by a large fractionation associated with a series of biosynthetic steps (Sessions et al., 1999). The relationship between source water and the isotopic composition of precipitation has been documented on large scale transect surveys of living plants, soils or lake sediments (Sachse et al., 2012), direct studies of plant waters in sub-tropical, dry climates (Feakins and Sessions, 2010a) and tropical, wet climates (Feakins et al., 2016). In the tropics, precipitation isotopic composition may respond to the "amount effect" with ^{2}H-enrichment (^{2}H-depletion) associated with drier (wetter) conditions (Lee et al., 2009). This effect can be amplified as leaf water ^{2}H-enrichment in dry climates can lead to smaller net fractionations (Feakins and Sessions, 2010a), resulting in further ^{2}H-enrichment of the plant wax. Terrestrial plant wax biomarkers preserved in geological records have thus been used to infer past wet/dry shifts, commonly using *n*-alkanes (Schefuß et al., 2005) and *n*-alkanoic acids (Tierney et al., 2008). Landscape vegetation dynamics can complicate the paleohydrological evidence that is recorded by plant waxes in some lake sediment archives (Douglas et al., 2012; Fornace et al., 2014). There are documented differences in biological factors between plant life form (e.g. trees, shrubs, graminoids) (Liu and Yang, 2008) and species (Sachse et al., 2012) due to leaf physiology (Smith and Freeman, 2006; Kahmen et al., 2013; Gao et al., 2015), phenology (Tipple et al., 2013) and biogeochemical pathway (Feakins and Sessions, 2010b). Therefore, plant wax reconstructions are ideally paired with evidence of plant communities in order to monitor vegetation change. This can be achieved by pairing carbon isotopic measurements on the same molecules (Nelson et al., 2013; Feakins et al., 2019), analyzing chain length distributions of particular compound classes (Fornace et al., 2014), and/or incorporating fossil pollen evidence of variations in taxa (Feakins, 2013; Sarkar et al., 2015; Lane et al., 2016; Nelson and Sachs, 2016; Freimuth et al., 2017).

In coastal environments, the source water accessed by mangroves may be a mixture of seawater and meteoric water, each of which has distinct δ^2H values. Salinity variations further complicate the recorded signal by altering the hydrogen isotopic fractionation between source water and plant lipids (Ladd and Sachs, 2012; Sachse et al., 2012). One approach to detect salinity changes in estuarine or lagoonal environments (Ladd and Sachs, 2015a, 2015b), has been to study the δ^2H values of taraxerol, the dominant sterol in *Rhizophora mangle* (red mangrove) leaves (Killops and Frewin, 1994; Koch et al., 2003). Field-based studies indicate that the net fractionation ($\varepsilon_{wax/w}$) between source water δ^2H and taraxerol δ^2H values increased 0.9 ± 0.2‰/ppt in salinity for *R. mangle* leaves in Micronesia (Ladd et al., 2015), and 0.5–1.0‰/ppt for *n*-alkanes extracted from three mangrove species growing across a salinity gradient within an Australian estuary (Ladd et al., 2015). In contrast, a laboratory-based cultivation study found a decrease in net fractionation with increased salinity (Park et al., 2019). Although uncertainties are large, some studies have attempted to deconvolve the changes in source water isotopic composition and salinity-dependent fractionations across salinity gradients by combining the signals from aquatic and mangrove biomarkers (Nelson and Sachs, 2016). More generally, mangrove inputs to sediments can be monitored through the use of both pollen and biomarker compounds (Versteegh et al., 2004). We thus propose to use the presence of pollen or mangrove biomarkers (e.g., taraxerol) as a diagnostic tool for inferring when mangrove inputs may modulate the signal recorded by *n*-alkyl plant wax biomarkers.

In pursuing this objective, we reconstruct regional hydroclimate variability from a 3000-year sediment record from Blackwood Sinkhole on Great Abaco Island in The Bahamas. Prior work on the bulk organic matter preserved within Blackwood Sinkhole has indicated shifts in the proportional inputs from both allochthonous material from the surrounding landscape (tropical, wet forest and mangrove marsh) and autochthonous productivity in the upper water column (Tamalavage et al., 2018). We develop a biomarker record from Blackwood Sinkhole including plant wax *n*-alkanoic acid hydrogen and carbon isotopic evidence for precipitation and ecological change over the last ~3000 years. We compare multi-proxy evidence from *n*-alkanoic acid, plant wax *n*-alkanes and mangrove-specific biomarkers, to previously published data on bulk organic signatures (Tamalavage et al., 2018) and preliminary pollen evidence for vegetation change (van Hengstum et al., 2016) to account for changes in the plant community and sediment deposition associated with the sinkhole. A paired pollen and plant wax approach provides solutions when working in small catchments with large ecological shifts (Fornace et al., 2016). In this case, the paired approach is used to screen, and attempt to correct for, mangrove biases and to develop a late Holocene precipitation isotope record for the northeastern Bahamas.

2. Study site

2.1. Blackwood sinkhole

Blackwood Sinkhole is located 220 m inland from the northeastern coast of Great Abaco Island on the Little Bahama Bank (26.79°N, 77.42°W; Fig. 1). This 32 m diameter, steep-sided sinkhole lake has a water depth of 33–38 m below sea level (mbsl), and a tidal range of ~1 m. A secondary, cylindrical karst feature (water depth ~46–61 mbsl) is connected to Blackwood Sinkhole through a cave tunnel at 32 mbsl. The sinkhole is bordered by significant mangrove wetland development on its eastern periphery (Fig. 1c), and is a groundwater-fed basin (proximal connection to the ocean) that receives no stream discharge. The sinkhole is hydrographically stratified, with surface salinity in the low oligohaline range (1.4 psu, most recent cast July 2019) and anoxic, saline groundwater from 15 to 40 mbsl.

We identified and analyzed biomarkers from a 1.22 m sediment core (BLWD-C2) previously collected in 2011 from Blackwood Sinkhole (van Hengstum et al., 2016). Radiocarbon dating of terrestrial plant macrofossils indicated a nearly constant sedimentation rate in the sinkhole over the last 3000 calibrated years before present (cal yrs BP, where present is 1950 CE; 0.3 to 0.6 mm/yr based on a Bayesian statistical approach, simple least squares linear regression: $r^2 = 0.99$, n = 11 dates) (van Hengstum et al., 2016; Tamalavage et al., 2018). Sediments are comprised of calcium carbonate and organic matter, with organic matter contributions from

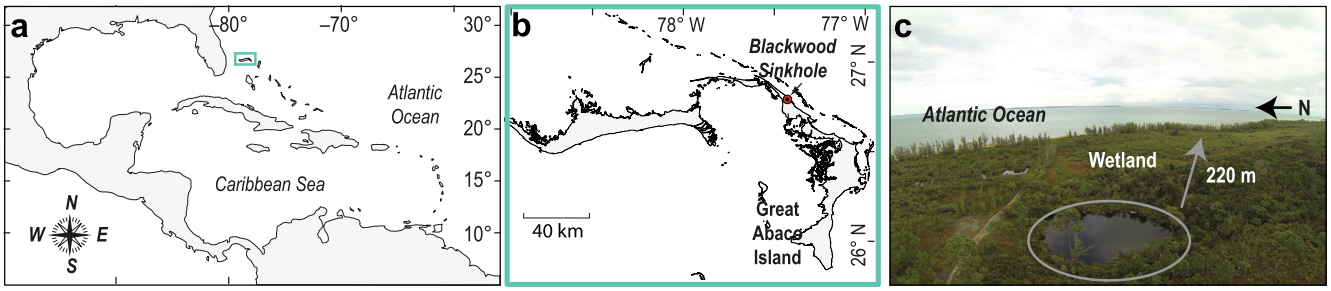

Fig. 1. Map of Blackwood Sinkhole on Great Abaco Island. (a) Caribbean region, green box expanded, (b) inset showing location of Blackwood Sinkhole, (c) photo of Blackwood Sinkhole (photo credit: Pete van Hengstum). (For interpretation of the references to color in this figure legend, the reader is referred to the web version of this article.) (For interpretation of the references to color in this figure legend, the reader is referred to the web version of this article.)

aquatic productivity and inputs from adjacent terrestrial and mangrove environments (Tamalavage et al., 2018).

2.2. Climate

The nearest meteorological station with rainfall isotopic data is Havana, Cuba (600 km southwest of Abaco Island), where Mean Annual Precipitation (MAP) is 1470 mm. Abaco Island has similar precipitation seasonality, with MAP of 1400 mm between 1951 and 1981 (Jury et al., 2007). Abaco has no record of isotopic data, therefore isotopic compositions from Havana will be used to infer likely δ^2H seasonality at Abaco. At the Havana station, the weighted MAP δ^2H is −11.8‰ (1σ = 8.0‰, 14 years, 2002–2016, IAEA/WMO, 2019; Fig. 2), and temperature seasonality is minimal (20.7–26.6 °C monthly mean). The wet season lasts from May to October (~195 mm/month, mean δ^2H −15.2‰), and the dry season lasts from November to April (~50 mm/month, mean δ^2H −3.5‰).

Latitudinal migration of the Intertropical Convergence Zone (ITCZ), pressure and geographic changes to the variability in the intensity and extent of the North Atlantic Subtropical High (NASH), and variability in the strength of the Caribbean Low Level Jet (CLLJ) all contribute to seasonal rainfall variability across the tropical North Atlantic region (Jury et al., 2007; Gamble and Curtis, 2008; Martin and Schumacher, 2011; Martinez et al., 2019). In the modern climate, rainfall across the Bahamian archipelago is highly sensitive to seasonal variability in the intensity (i.e., stronger being higher central pressure), and geographic position of the NASH. For example, (Hasanean, 2004) determined that NASH intensity was greatest (weakest) during boreal summer (winter) from 1960 to 1990 CE using NCEP-NCAR reanalysis data gridded at 2.5° x 2.5°. It has been further determined that the geographic position of the westward margin of the NASH regulates rainfall on the Caribbean and SE United States (Li et al., 2011; Li et al., 2012).

In order to understand the linkages between precipitation isotopes and atmospheric conditions, we identify the 2.5% of years (75 total years) with the most ^2H-enriched and ^2H-depleted rainfall in three forced transient simulations of the time period 850–1849 CE (including all external forcing factors—volcanic, greenhouse gas, solar) with the isotope enabled Community Earth System Model (iCESM) (Brady et al., 2019). While the iCESM struggles to reproduce the observed seasonal cycle of δ^2H (Supplemental Information, Fig. S1g) and precipitation (Supplemental Information, Fig. S1h) at Havana, Cuba, with an exaggerated midsummer drought and a mean offset, the difference between wet and dry years appear to be well captured by the model (Supplemental Information Fig. S1a-c versus Fig. S1d-f). Ideally, forced transient simulations covering the same time period as the reconstruction would be available for this analysis. While such simulations do not exist, the boundary conditions are largely stable (except on longer than centennial timescales) in the late Holocene and thus interannual variability should be similar for sub samples of the reconstructed time period. Together these results suggest that iCESM simulations will be useful for interpreting the regional-to-large scale climate dynamics underlying local variability in δ^2H.

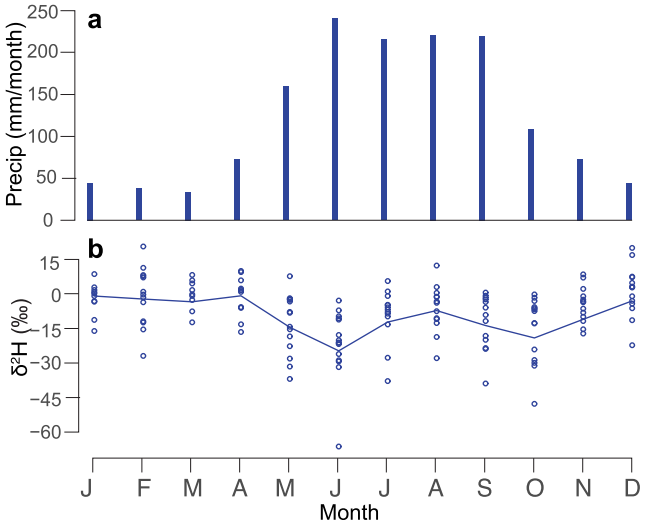

Fig. 2. Precipitation amount and hydrogen isotopic composition, showing (a) monthly mean precipitation amount, and (b) monthly measurements and weighted climatological mean δ^2H precipitation, from Havana, Cuba (Centro de Proteccion e Higiene de la Radiacion; CPHR) based on 154 measurements taken from 2002 to 2016 (IAEA/WMO, 2019). The rainy season (May-October; mean δ^2H – 15.2‰) is ~12‰ ^2H-depleted relative to the dry season (November-April; mean −3.5‰).

In the composite of the 1% of most ^2H-enriched years, we find the NASH intensifies and expands (Fig. 3a), suppressing convection over the Caribbean. At the same time, a stronger Caribbean Low Level Jet (CLLJ) increases moisture export (divergence) away from the Caribbean. Together these conditions bring drier conditions across a large area of the Caribbean (Fig. 3c). Conversely, in the most ^2H-depleted years, the NASH is weak (i.e. lower central pressure) and contracted (i.e. western boundary as defined by the 850 mbar is displaced further to the East) (Fig. 3b), the CLLJ is weak, and there are wetter conditions across the Caribbean. Filtering to isolate multidecadal (the nominal resolution of the reconstructions—see Methods) and longer timescale variability produces similar, though expectedly muted differences between ^2H-depleted and enriched periods. The same dynamics that are associated with isotopic variability over The Bahamas have been shown to also control the large scale patterns of hydroclimate variability across the Mesoamerican-Caribbean region (Bhattacharya and Coats, 2020).

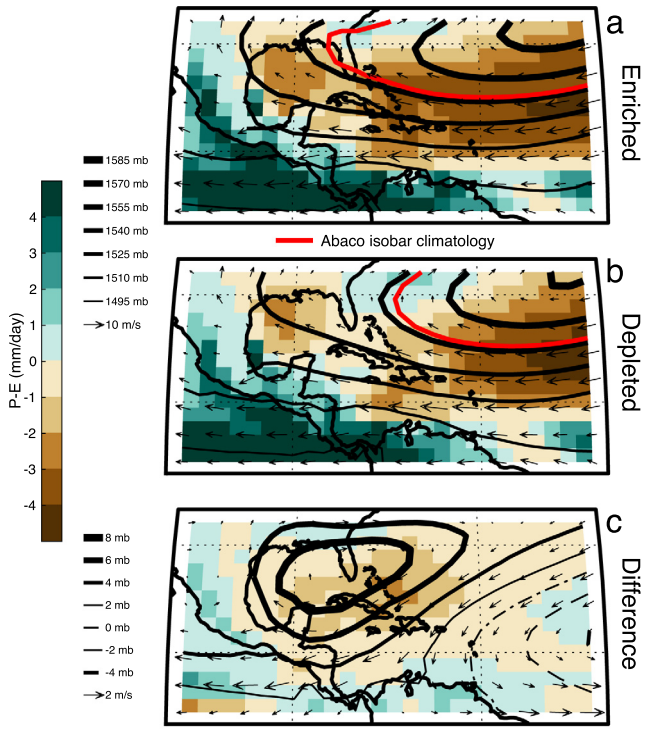

Fig. 3. Comparison of May-October precipitation minus evaporation (P-E, color), 850 mb wind (vectors), and 850 mb geopotential height (contours) highlighting the climatological isobar that sits over Abaco (red line) for the 2.5% most a) ^{2}H-enriched and b) ^{2}H-depleted rainfall years, and the c) difference, near Abaco (average of 40 years total) from four isotope enabled Community Earth System Model last millennium simulations (iCESM—forced transient between 850 and 1850 CE). The most ^{2}H-enriched and ^{2}H-depleted years were calculated for the average of all spatial grid points within 300 km of Abaco (26.79°N, 77.42°W). ^{2}H-enriched rainfall over Abaco corresponds to an expanded NASH (see red line) and stronger CLLJ, which lead to greater local atmospheric stability and greater moisture export out of the Carribean, respectively, and ^{2}H-depleted rainfall corresponds to a contracted NASH and weaker CLLJ. (For interpretation of the references to color in this figure legend, the reader is referred to the web version of this article.)

3. Methods

3.1. Lipid extraction

Previously analyzed pollen samples were collected every 10 mm, with each sample integrating 5 mm of core and up to ~12 years of inputs (Fall unpublished data; van Hengstum et al., 2016; Tamalavage et al., 2018). Sediment sub-samples were collected for biomarker analysis every 30 mm (~every 72 years) with each sample integrating 10 mm of core, or ~24 years of inputs, while 17 biomarker samples were screened downcore for sterol compounds (Supplemental Information, Fig. S2). Samples for biomarker analysis were freeze dried and homogenized with a mortar and pestle. Dry, powdered sediment samples (about 1–2 gdw) were extracted with an Accelerated Solvent Extraction system (ASE 350®, DIONEX) with 9:1 ratio of dichloromethane (DCM): methanol (MeOH) at 100 °C and 1500 psi (2 × 15-min). The extract was separated using column chromatography (5 cm × 40 mm Pasteur pipette, NH_2 Sepra brand bulk packing, 60 Å), eluting with 2:1 DCM:isopropanol, followed by 4% HCO_2H in diethyl ether, yielding neutral and acid fractions respectively. The neutral fraction was separated by column chromatography (5 cm × 40 mm Pasteur pipette, 5% water-deactivated silica gel, 100–200 mesh) by eluting with hexanes to separate *n*-alkanes from the rest of the neutral fraction (eluted with DCM and methanol, including sterols, hence "sterol fraction"). Sulfur was removed from the *n*-alkane fraction by eluting over activated copper filings. The acid fraction containing *n*-alkanoic acids was methylated with 5% HCl and 95% MeOH (with methyl group of known isotopic composition: δ^{2}H −186.9‰ ± 3.7; 1σ; δ^{13}C −24.7‰ ± 0.2) at 70 °C for 12 h to yield corresponding fatty acid methyl esters (FAMEs). Measured FAME isotopic compositions were corrected for the added methyl group to yield the isotopic composition of the original fatty acid by mass balance. Excess milliQ water was added to the hydrolyzed products, and the lipids were partitioned into hexane and dried by passing through anhydrous Na_2SO_4. Lipids were further purified using column chromatography (5 cm × 40 mm Pasteur pipette, 5% water-deactivated silica gel, 100–200 mesh), eluting with hexane first and then with DCM to isolate the FAME fraction.

3.2. Biomarker identification and quantification

We identified the *n*-alkanes and *n*-alkanoic acids (the latter as fatty acid methyl esters, FAME) by gas chromatography (GC) mass spectrometry (MS) and quantified these compounds by a flame ionization detector (FID), using an Agilent GC-MSD/FID. *n*-Alkanes and FAME fractions were dissolved in hexane and injected via a split/splitless inlet in splitless mode, to a capillary column (Rxi®-5ms 30 m × 0.25 mm, film thickness 0.25 μm). Quantification was achieved using an in-house standard comprised of a mixture of four *n*-alkanes and three *n*-alkanoic acid methyl esters of varied and known concentration, with the linear calibrations determined separately for the two compound classes. The *n*-alkanoic acid concentrations are reported relative to the dry weight of the sediment, with the *n*-alkane concentrations determined for a subset.

We calculate the following equations using the range of *n*=C_{24}-C_{30} for *n*-alkanoic acids. We calculate the carbon preference index (CPI), or even over odd carbon chain length preference as:

$$CPI = 2\Sigma C_n/(\Sigma C_{n-1} + \Sigma C_{n+1}) \quad (1)$$

We calculate the average chaing length (ACL), the weighted average accounting for concentration (Cn) of each compound (*n*) as:

$$ACL = \Sigma(C_n n)/\Sigma C_n \quad (2)$$

The *n*-alkanoic acid concentrations were summed as:

$$\Sigma_{acids} = \Sigma_i^n [C_n] \quad (3)$$

where n indicates the chain length *n*=C_{24}-C_{30} for *n*-alkanoic acids. We similarly calculated the same ratios for the *n*-alkanes using the *n* = C_{27}-C_{33} range. In addition, we report the modal chain lengths of each compound class.

We studied the sterol fraction of a subset of the samples (*n* = 17) to identify biomarkers for mangroves, specifically taraxerol. Samples were derivatized using 25 μl of N,O-Bis(trimethylsilyl)trifluoroacetamide (BSTFA) with trimethylchlorosilane trimethylsilyl chloride (TMCS; 99:1 v/v) and 100 μl of pyridine, reacting at 70 °C for 20 min. Samples were dissolved in DCM (375 μl) and analysed by GC–MS/FID. Compound identification was made by comparison of MS *m/z* spectra to those in the literature (Killops and Frewin, 1994). Sterols were quantified by comparison of FID peak area for the analyte relative to that of a four-point in-house linear calibration of cholestane. In addition, we calculated taraxerol/$\Sigma_{alkanes}$ to account for concentration changes such as clastic dilution of both plant components to the sedimentary matrix and to reveal relative changes in mangrove inputs.

3.3. Compound-specific hydrogen and carbon isotopic analysis

Compound-specific hydrogen isotopic values were obtained using gas chromatography isotope ratio mass spectrometry (GC-

IRMS). We used a Thermo Scientific Trace gas chromatograph equipped with a Rxi-5 ms column (30 m × 0.25 mm, film thickness 0.25 μm) and a programmable temperature vaporizing (PTV) injector. Injections were performed via the PTV inlet operated in solvent split mode, whereby the solvent was evaporated at 60 °C in split mode, then the temperature raised to 280 °C for transfer of analytes to the GC column in splitless mode. The GC was connected via a GC Isolink with pyrolysis furnace (at 1400 °C) via a Conflo IV interface to a DeltaVPlus isotope ratio mass spectrometer. To check for linearity, the H_3^+ factor was measured daily and remained close to 4 ppm mV^{-1} (across 1–8 V); for CO_2 the standard deviation of reference pulses was better than 0.9‰. Reference peaks of H_2 or CO_2 were co-injected during the course of a GC-IRMS run; two were used for standardization. Samples were interspersed with standard compound mixtures of known isotopic composition, with several standards run per day. The results are reported using conventional delta notation (δ^2H and $\delta^{13}C$ in permil: ‰),

$$\delta = (R_{sample} - R_{standard})/R_{standard} \quad (4)$$

in which R is $^2H/^1H$ or $^{13}C/^{12}C$, respectively.

Data were normalized to the VSMOW/SLAP hydrogen isotopic scale by comparing with an external standard (A3 mix for samples run before August 2017; A6 mix for samples run after late July 2017) obtained from A. Schimmelmann (Indiana University) containing 15 *n*-alkane compounds (C_{16} to C_{30}), with δ^2H values spanning −227 to −46‰ for A3 mix and −256 to −17‰ for A6 mix; and $\delta^{13}C$ values spanning −33.37 to −28.61‰ for A3 mix and −33.97 to −26.15‰ for A6 mix. The RMS error determined by replicate measurements of the standard across the course of analyses was 3.7‰ for δ^2H and 0.21‰ for $\delta^{13}C$. FAMEs were corrected for H or C of the methyl group added in methylation by mass balance to yield the δ^2H and $\delta^{13}C$ of the corresponding fatty acid (following the methods of (Lee et al., 2017)).

Isotopic fractionations between δ_a and δ_b, as ^2H-depletion factors ($\varepsilon_{a/b}$), were calculated with the following equation:

$$\varepsilon_{a/b} = \alpha_{a/b} - 1 = [(\delta_a + 1)/(\delta_b + 1)] - 1 \quad (7)$$

4. Results

4.1. Plant wax abundance

We quantified *n*-alkanoic acids with carbon chain lengths of 24 (0.7 to 14.6 μg/g), 26 (1.9 to 45.7 μg/g), 28 (1.7 to 102.7 μg/g) and 30 (0.4 to 19 μg/g). Overall, the modal chain length was 28, with an ACL of 27 ± 0.4 (1σ, n = 67). The average CPI was 10 ± 5, indicating input from terrestrial higher plants (Freeman and Pancost, 2013). We found two main patterns in chain length abundance throughout the ~3000-year record (Fig. 4a, c): C_{28} was the modal homolog overall, and it had a higher relative abundance (C_{28}/ΣC_{24}:C_{30}) between 2950 to 850 cal yrs BP (mean 45%), compared to 28% in the last 850 years (Fig. 4b).

We quantified the C_{26} to C_{33} *n*-alkane concentrations in 14 samples at low resolution through the core. The abundance of C_{27} *n*-alkanes were 0.2 to 12 μg/g, C_{29} *n*-alkanes were 0.7 to 7.8 μg/g, C_{31} *n*-alkanes were 1.2 to 18.6 μg/g, and C_{33} *n*-alkanes were 0.5 to 8.2 μg/g (Fig. 4d). The mean ACL was 30.6 ± 0.6 (1σ, n = 14) and mean CPI was 13 ± 5 (1σ, n = 14). C_{31} is the modal chain length and abundance distributions did not differ significantly in the comparison before and after 850 cal yrs BP (Fig. 4c), but note the small sample size in the *n*-alkane dataset relative to the *n*-alkanoic acid analyses.

We found detectable taraxerol in 11 of the 17 samples screened for mangrove-derived triterpenol biomarkers (*n* = 17). Taraxerol concentrations range from 0.4 to 11.2 μg/g (mean = 4.1 μg/g, σ = 3.8 μg/g, n = 11). The proportion of mangrove biomarkers to *n*-alkanes, taraxerol/$\Sigma_{alkanes}$ (calculated for 11 samples) ranged from 0.04 to 3.08, with high values (>0.5) only after 850 cal yrs BP (Fig. 6d).

4.2. Hydrogen isotopes

We measured the δ^2H values of *n*-alkanoic acids, which ranged from −157 to −110‰ (mean = −136‰, 1σ = 14‰, n = 29) for C_{24}, −160 to −103‰ (mean = −124‰, 1σ = 13‰, n = 55) for C_{26}, −158 to −99‰ (mean = −121‰, 1σ = 16‰, n = 57) for C_{28}, and −149 to −99‰ (mean = −129‰, 1σ = 15‰, n = 28) for C_{30} through the core (Fig. 5a). The C_{28} *n*-alkanoic acid is selected to describe downcore variations as it is considered representative of inputs from long-chained terrestrial plants (Freeman and Pancost, 2013), and is abundant in tropical forests (Feakins et al., 2016). Values of δ^2H_{28} span ~50‰ throughout the record. There is a trend from higher δ^2H_{28} values (mean = −112‰, 1σ = 9‰, maximum value = −99‰) from 2950 to 850 cal yrs BP to lower δ^2H_{28} values starting at approximately 850 cal yrs BP (mean = −143‰, 1σ = 8‰, minimum value = −158‰) (Fig. 5b).

4.3. Carbon isotopes

For a subset of samples analyzed for hydrogen isotopes (Fig. 6a), $\delta^{13}C_{28}$ values were determined for 18 samples downcore (Fig. 6b). Values of $\delta^{13}C$ for each chain length ranged from −42 to −28‰ (mean = −36‰, 1σ = 4‰) for C_{24}, −43 to −29‰ (mean = −38‰, 1σ = 4‰) for C_{26}, −45 to −30‰ (mean = −38‰, 1σ = 5‰) for C_{28}, and −45 to −30‰ (mean = −34‰, 1σ = 4‰) for C_{30}. These values are within the expected range for C_3 angiosperms (Chikaraishi and Naraoka, 2007; Freimuth et al., 2017; Wu et al., 2017). $\delta^{13}C_{28}$ reveals little variability from 2150 to 850 cal yrs BP (mean = −41‰, 1σ = 2‰), but $\delta^{13}C_{28}$ values are variable and more enriched from 850 cal yrs BP (mean = −35‰, 1σ = 5‰) to the present. There are two shifts to more ^{13}C-enriched values after 850 and 370 cal yrs BP, at the same time as shifts in δD_{28} (Fig. 5).

5. Discussion

5.1. Vegetation community and plant wax inputs to the sinkhole

Before interpreting the downcore variations in plant wax hydrogen isotopic composition, we must consider evidence for changing vegetation (Fig. 6e–h). Pollen spectra indicate a major change in the vegetation community after 850 cal yrs BP, as tropical hardwoods and palms (*Myrtaceae* and *Arecaceae*) are replaced by pines (*Pinus*) and mangrove taxa (*Laguncularia racemosa* and *Conocarpus erectus*) (Fall unpublished data; van Hengstum et al., 2016; Tamalavage et al., 2018). *C. erectus* and *L. racemosa* are the dominant mangrove taxa represented in the pollen record, whereas pollen from both *Rhizophora mangle* (prolific pollen producer) and *Avicennia* (poor pollen producer) (Urrego et al., 2009) is very low throughout the record. The presence of taraxerol identified within this study at low resolution might seem to suggest that *R. mangle* is present on the landscape, as taraxerol dominates the lipid composition of *R. mangle* leaves (Killops and Frewin, 1994; Versteegh et al., 2004), but pollen abundance for *R. mangle* is low and modern distributions are mostly found on muddy shores and brackish environments on the leeward sides of the islands. Alternatively, the identified sterols may derive from other mangrove species, consistent with studies of *Avicennia* and *Laguncularia* by Koch et al. (2003). Thus, the presence of triterpenols (taraxerol) corroborate pollen evidence indicating an increase in mangrove plants on the adjacent landscape after 850 cal yrs BP (Fig. 6d).

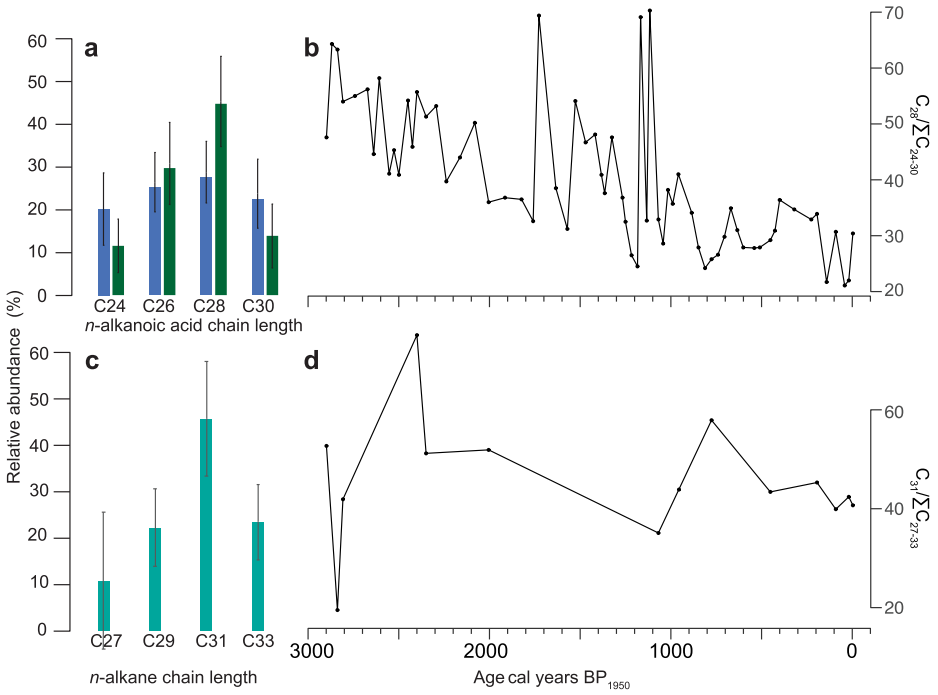

Fig. 4. (a) Chain length abundance of *n*-alkanoic acids, separated into two groupings (850 cal yrs BP, blue, to present, and 850–3000 cal yrs BP, green), (b) relative abundance of C_{28} *n*-alkanoic acid with time, (c) abundance distribution of *n*-alkanes, and (d) relative abundance of C_{31} *n*-alkane with time. (For interpretation of the references to color in this figure legend the reader is referred to the web version of this article.)

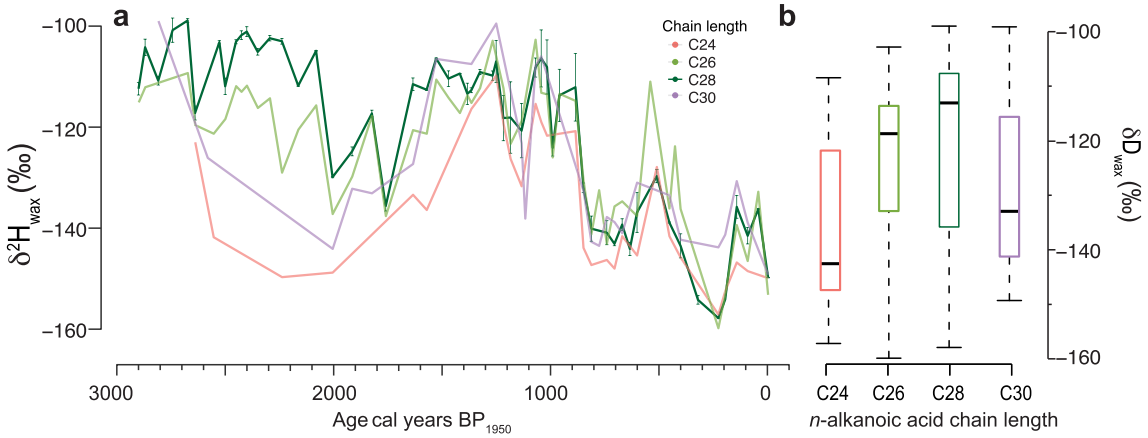

Fig. 5. Hydrogen isotopic measurements for *n*-alkanoic acids showing (a) downcore δ^2H values for the late Holocene and (b) δ^2H values by chain length for the even chain length C_{24} to C_{28} *n*-alkanoic acids, showing median (thick line), interquartile range (box) and range (whiskers).

$\delta^{13}C$ and C:N ratios measured on bulk organic matter deposited within the basin confirm an expansion of wetland on the adjacent karst landscape (Tamalavage et al., 2018). Within the plant wax biomarkers, we find that the C_{28} *n*-alkanoic acid relative abundance decreases from 45% to 28% at 850 cal yrs BP (Fig. 4a). This could indicate a change in plant wax community inputs, or a change in degradation or microbial activity (Li et al., 2018). Within this time period, plant wax $\delta^{13}C$ values increase with the appearance of pines and mangroves (Fig. 6c), which is consistent with fractionations in conifers as well as in more open habitats (Diefendorf and Freimuth, 2017).

Plant wax hydrogen isotopic compositions become more ^2H-depleted after 850 cal yrs BP, specifically from 850 to 600 cal yrs BP (Fig. 6b), which coincides with an increase in mangrove pollen from 890 to 680 cal yrs BP (Fig. 6e) and lower proportions of pine (Fig. 6f), with a second phase of ^2H-depletion from 450 to 150 cal yrs BP. The shifts to more ^2H-depleted values are likely dominated by the greater fractionations associated with increased salinity and mangrove plant inputs (Ladd and Sachs, 2012). The simultaneous increase in $\delta^{13}C$ values and depleted δ^2H values could be due to discrimination associated with decreasing stomatal conductance under increasingly saline or water-stressed conditions (Farquhar et al., 1982; Lin and Sternberg, 1992). There will be less discrimination against ^{13}C under these conditions, and resultant carbon will be enriched as the CO_2 pool within the leaf is increased in $\delta^{13}C$ (Ladd and Sachs, 2013).

5.2. Correcting for mangrove inputs

Prior work has shown that the emplacement of the adjacent wetland occurred after ~1350 cal yrs BP, based on the basal age of a wetland peat core (van Hengstum et al., 2016). However,

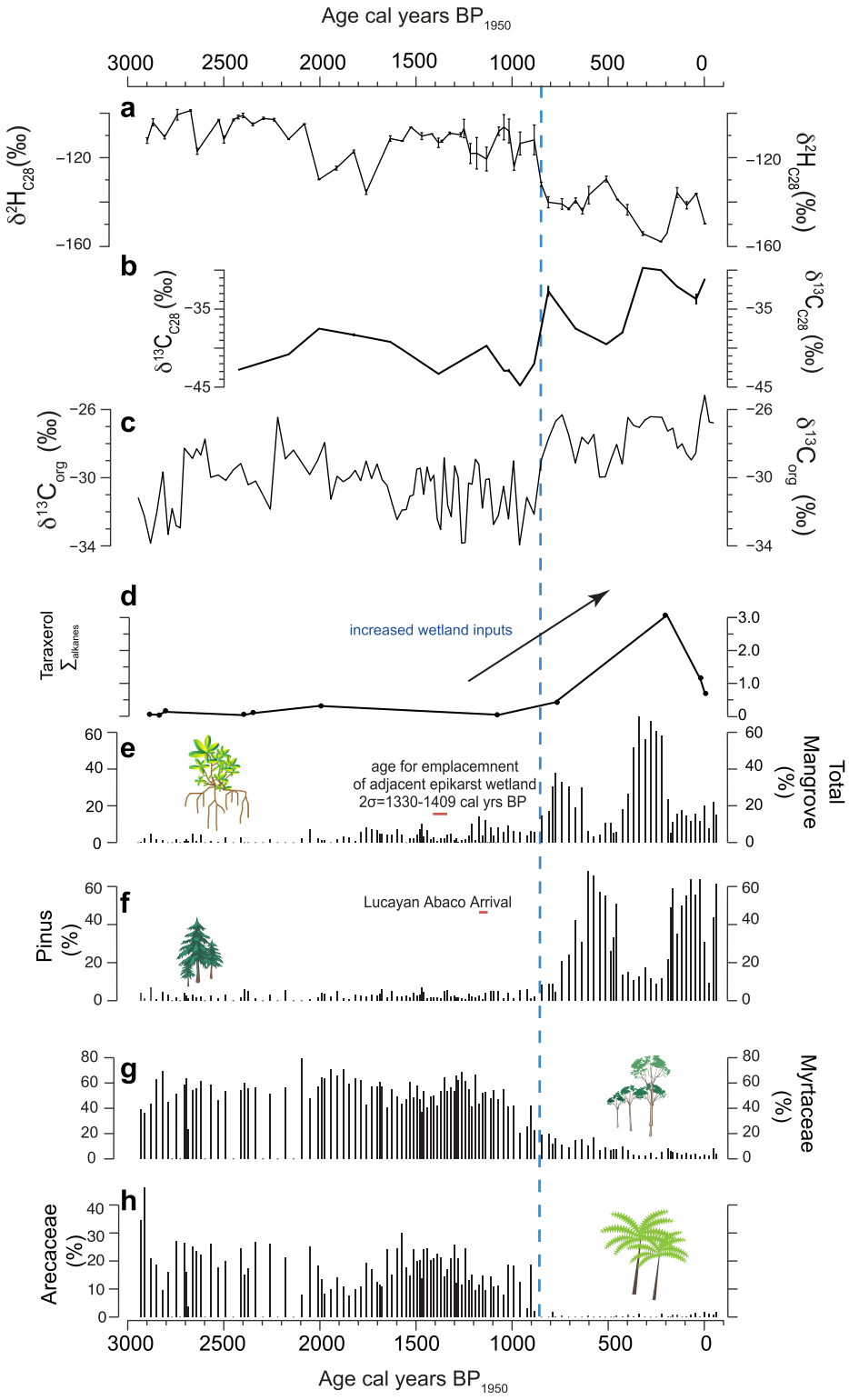

Fig. 6. Comparison of geochemical results from BLWD-C2, where 0 is 1950 CE, (a) downcore δ^2H_{28} values, (b) downcore $\delta^{13}C_{28}$ values, (c) $\delta^{13}C_{org}$ for BLWD-C2 (Tamalavage et al., 2018) (d) downcore taraxerol/$\Sigma_{alkanes}$, (e–h) Pollen results from BLWD-C2 (Fall, unpublished; van Hengstum et al., 2016; Tamalavage et al., 2018; van Hengstum et al., 2018), and direct evidence of human occupation on Abaco (Steadman et al., 2007; Sullivan et al., 2020). The change in the vegetation community as detected by pollen also marks a major transition in the plant biomarker signals at about 850 cal yrs BP (blue dashed line). (For interpretation of the references to color in this figure legend the reader is referred to the web version of this article.)

changes in the organic matter in sinkhole sediments are indicated by $\delta^{13}C$ values in the bulk organic matter only after ~1000 cal yrs BP (Tamalavage et al., 2018). Mangrove pollen first appears in abundance after 850 cal yr BP (Fig. 6), suggesting the start of the mangrove influence on plant wax records in the core.

Given the covariation between mangrove pollen and plant wax δ^2H, we attempt to correct for the influence of mangroves to extract the signal of terrestrial vegetation and thus precipitation δ^2H. Due to uneven sampling between pollen and biomarker sampling and analysis (Supplementary Information, Fig. S2), mangrove

pollen and plant wax δ^2H were interpolated to evenly spaced intervals (1 cm). As triterpenols were studied at low resolution, they are used as a cross check on the pollen findings and therefore not used for the mangrove correction.

We determined an empirical relationship between δ^2H_{28} and total mangrove pollen (Fig. 7a), during the presence of mangrove (mostly > 10% mangrove pollen) from 850 cal yrs BP to the present (Fig. 7b). In that interval, we found a significant negative correlation ($r = -0.77$, $p < 0.05$) (Fig. 7a), using non-parametric methods that account for serial correlation (Ebisuzaki, 1997). This correlation implies that mangrove inputs explain about 56% of the variance. If we assume the linear fit describes the mangrove influence and that the remainder of the variance (residual) is due to terrestrial plant wax inputs primarily responding to hydrological variability (δ^2H_{precip}), then we can use the empirical regression of the linear fit to remove the mangrove influence. As measured plant waxes from 850 cal years BP to the present are comprised by both mangrove and terrestrial plant inputs, this offers a pragmatic approach to mangrove correction based on the empirical relationship over time, which incorporates the strong negative correlation and mechanistic basis for that relationship (Ladd et al., 2012). Principal uncertainties are related to inter-plant and inter-species variations in hydrogen isotope fractionations such as: species and salinity effects that are too challenging to quantify without additional data, unconstrained connections between pollen abundance and the amount of plant wax inputs from mangroves, as well as minor uncertainties related to uncertainties on analytical determinations of δ^2H values and pollen counts.

We used the mangrove pollen abundances to predict the mangrove contributed plant wax δ^2H ($\delta^2H_{m\text{-}pred}$):

$$\delta^2H_{m-pred} = mangrovepollen(\%) * (--0.3053) + (--134.77) \quad (8)$$

and we corrected the measured δ^2H_{28} values to yield the mangrove-corrected value δ^2H_{corr} (Fig. 7b), which is approximated by:

$$\delta^2H_{corr} = \delta^2H_{measured} - -mangrovepollen(\%) * (--0.3053) \quad (9)$$

Mangrove corrected values are more enriched than measured values, especially during intervals of increased mangrove pollen (~850–680 cal yrs BP; 520–280 cal yrs BP). During those intervals, δ^2H_{corr} ranges from −136 to −126‰, compared to δ^2H_{28} of −154 to −130‰. The correction reduces the variance, with δ^2H_{corr} values for the last 850 cal yrs BP falling more closely within the measured range of δ^2H_{28} from ~3000 to 2000 cal yrs BP, when mangrove inputs were minimal. This pollen-based mangrove correction does not explicitly account for salinity, but the approach implicitly assumes that an increase in mangrove inputs corresponds to an increase in source water salinity, and uses the regression between mangrove pollen (%) and δ^2H to remove that combined mangrove and salinity effect. However, this relationship may be confounded by changes in precipitation δ^2H or changes in salinity independent of mangrove pollen flux. If we consider the increasing fractionation with increasing salinity reported in field studies elsewhere ~−1‰/psu (Ladd and Sachs, 2012, 2015a, 2015b; He et al., 2017), the observed decline in δ^2H values is on the order of −30‰ associated with the mangrove pollen increase. This could be explained by a shift from freshwater to seawater salinities, and would suggest very little change in precipitation δ^2H as the mangroves expanded.

5.3. Estimating precipitation isotopic composition

Net fractionations ($\varepsilon_{28/precip}$) were calculated between the δ^2H_{28} value for the sediment closest to the core top (at 2.5 cm or +50 yrs BP, or 2000 CE) and weighted mean annual δ^2H_{precip} from the closest GNIP station in Havana, Cuba (2002–2016), in sediments that have ~20% mangrove pollen. Calculated $\varepsilon_{28/precip}$ is −139‰, which is slightly higher than global estimates of fractionation, as expected given the partial mangrove influence in this horizon. In comparison, global estimates for C_{29} *n*-alkanes for angiosperms are −113‰ ± 30‰ (Sachse et al., 2012), and dual compound class studies of tropical forests reporting fractionations are −129‰ ± 2‰ for C_{29} n-alkanes and −121‰ ± 3‰ for C_{28} *n*-alkanoic acids (Feakins et al., 2016). We use the tropical forest fractionation for C_{28} *n*-alkanoic acids for predictions of $\delta^2H_{precip\text{-}raw}$, which is thought to be appropriate for the majority of the record that is not mangrove-influenced. For the mangrove-influenced horizons, we apply the pollen-corrected approach, which results in a varying fractionation that encompasses the coretop calculated fractionation ($\varepsilon_{28/precip}$ = −134‰), and also predicts a larger fractionation for the sediments with up to 60% mangrove pollen. After correcting for mangrove inputs, we obtain estimates of $\delta^2H_{precip\text{-}corr}$ from −18.2 to + 25‰ throughout the last 2950 years (Fig. 8a).

As intended, the isotopic range of the $\delta^2H_{precip\text{-}corr}$ (58‰) is smaller than the range of the $\delta^2H_{precip\text{-}raw}$ without mangrove correction (67‰). In comparison, the Havana CPHR GNIP station has a recorded range of monthly totals from −66.3 to + 20.6‰ (Fig. 2), although the mean climatological seasonality is much smaller at −15.2 to – 3.5‰. Although all values in the non-mangrove corrected record are theoretically possible within a rainfall event, it would be surprising to obtain such a depleted signal in the sediments which represent multidecadal (~60 yr) averages (Fig. 2b). Therefore, the mangrove-corrected $\delta^2H_{precip\text{-}corr}$ likely better represents past rainfall variations, when mangroves are present. Although calculated values of $\delta^2H_{precip\text{-}corr}$ are plausible, the magnitude of the variation is large and corrected values should be interpreted cautiously given the imperfect nature of the mangrove correction attempted here.

Uncertainties of measured δ^2H_{28} values include <2‰ instrument precision (1σ, sample replicates), 4‰calibration accuracy, and uncertainties on the δ^2H_{28} /pollen regression are 5‰. Many additional uncertainties in this application cannot be readily quantified. One uncertainty derives from the different depths of pollen and biomarker samples, and resulting uncertainty in the correlation exercise. In terms of ecosystem processes, perhaps the largest of the uncertainties on $\delta^2H_{precip\text{-}corr}$ derives from the likely differences between the proportional production of pollen among the different plant species and that of their wax productivity. Another concern is additional salinity-induced fractionations within the mangroves. Our method assumes that on multi-decadal timescales, higher salinities would correspond to higher proportions of mangroves, but salinity can vary on shorter timescales, which is presently unconstrained. Uncertainty on the mean tropical forest fractionation is 3‰ (s.e.m) (Feakins et al., 2016), however, the epsilon for this Caribbean ecosystem has not yet been determined rigorously. While it is not possible to quantify unknown uncertainties, a 10-20‰ uncertainty on the mangrove-corrected estimate is plausible.

Another concern is that the reconstructed values are more enriched than would be expected, given the observed to the seasonal cycle of rainfall and the multi-decadal averaging in sediments. This further suggests a bias and that the epsilon should likely be smaller than the coretop or tropical forest value. Fractionations as small as −93‰ have been noted in sub-humid and semi-arid southern California (Feakins et al., 2014) and if this also applied in dry times in the Caribbean, it could shift precipitation reconstructions by up to −30‰. Alternatively, plants could have a strong growth seasonality or be accessing a lens of evaporatively-enriched water stored in the karst. Elsewhere, a similar issue of enriched reconstructions was noted by Taylor et al. (2020) in Costa Rica, where their reconstructed δ^2H_{precip} values

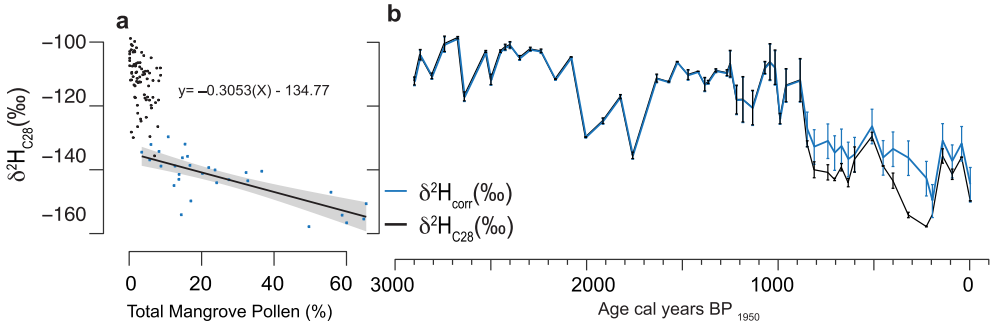

Fig. 7. (a) Mangrove pollen (*Laguncularia, Avicennia, Rhizophora, Conocarpus erectus*) versus δ^2H_{28} values downcore, interpolated at 1 cm increments, (b) Downcore δ^2H_{28} values measured (black line) and mangrove-corrected (blue line). (For interpretation of the references to color in this figure legend the reader is referred to the web version of this article.)

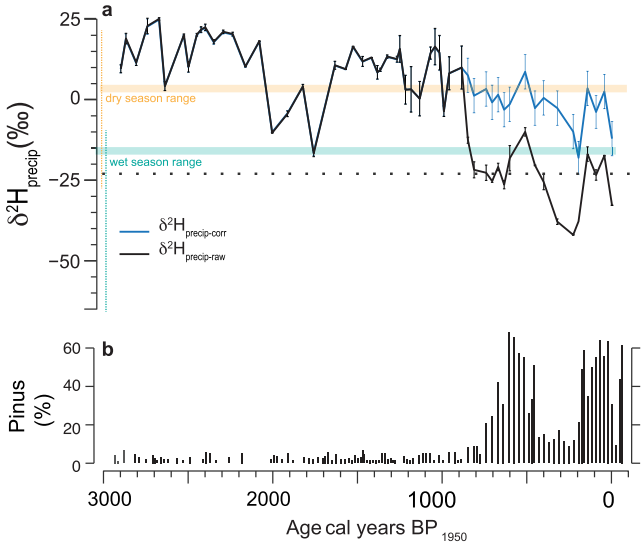

Fig. 8. (a) Precipitation isotopic reconstructions based on measured plant wax ($\delta^2H_{precip\text{-}raw}$ black line) and after mangrove-correction ($\delta^2H_{precip\text{-}corr}$, blue line). Horizontal thick, colored lines represent mean dry (orange) and wet (teal) season values recorded at the nearby Havana, Cuba GNIP station, and vertical lines show the range of monthly precipitation across 14 years (2002-2016); (b) pine pollen (Fall, unpublished; van Hengstum et al., 2016). (For interpretation of the references to color in this figure legend the reader is referred to the web version of this article.)

based on n-alkanes are more enriched than the seasonal GNIP cycle, suggesting that plants were using more isotopically heavy water throughout the year, rather than summertime rainfall. These questions suggest that local calibrations of plant water isotope systematics will represent an important future development.

5.4. Regional hydroclimate

At Blackwood Sinkhole on Abaco, the vegetation is relatively stable from 2950 to 850 cal yrs BP (Fig. 6e–h), providing confidence in precipitation isotopic reconstructions. Generally, high δ^2H values from 2950 to 850 cal yrs BP would imply an expanded NASH and increased local subsidence, likely accompanied by dry conditions on Abaco island (with $\delta^2H_{precip\text{-}corr}$ values similar to the dry season within the instrumental record; Fig. 8a). If we set this record in context with other reconstructions from across the Caribbean region (Fig. 9), we see some shared patterns. The dry period from 2950 to 2100 cal yrs BP (Fig. 9a, yellow shading) corresponds to evidence for aridity across the Caribbean between ~3300 and 2500 cal yrs BP (Berman and Pearsall, 2000; Fensterer et al., 2013; Gregory et al., 2015), including a speleothem record from

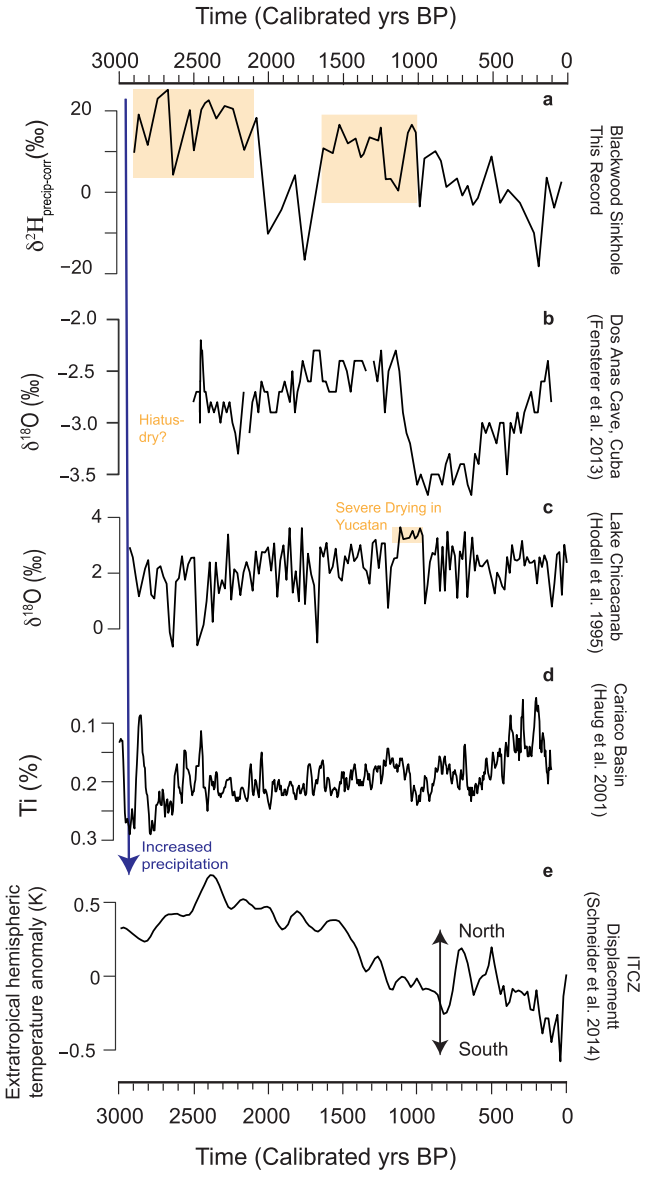

Fig. 9. Regional paleoclimate comparison: (a) reconstructed $\delta^2H_{precip\text{-}corr}$ from this study, (yellow shading denotes inferred aridity); (b) $\delta^{18}O$ values from a nearby speleothem in Dos Anas Cave, Cuba (Fensterer et al., 2013), yellow bar indicates a hiatus likely due to drought; (c) $\delta^{18}O$ values from the gastropod *Pyrgophorus coronatus* recorded within Lake Chichancanab, Mexico; (d) Ti record of terrestrial runoff from the Cariaco Basin (Haug et al., 2001); and (e) the Northern-to Southern Hemisphere Temperature anomaly (Schneider et al., 2014) interpreted as a measure of ITCZ displacement as indicated by the arrow. (For interpretation of the references to color in this figure legend, the reader is referred to the web version of this article.)

Cuba (Fig. 9b) and low runoff from Venezuela to the Cariaco Basin (Fig. 9d). On Abaco, a marine sapropel within No Man's Land Sinkhole similarly suggests low rainfall amounts from ~3300 to 2500 cal yrs BP, with increased rainfall after 2500 cal yrs BP (van Hengstum et al., 2018). On Abaco, we find a shift to more depleted δ^2H_{precip} from ~2100 to ~1700 cal yrs BP (Fig. 9a), perhaps linked to a contracted NASH and more rainfall on Abaco (Fig. 2), which is partly consistent with the No Man's Land Sinkhole record (van Hengstum et al., 2018). From 1700 to 900 cal yrs BP, generally high $\delta^2H_{precip\text{-}corr}$ values (Fig. 9a, yellow shading) suggest a period of increased aridity in the Northern Caribbean. Arid conditions around 1230 cal yrs BP may relate to onset of the "Terminal Classic Drought" documented within the Yucatan Peninsula, Mexico (Curtis et al., 1998; Hodell et al., 2005; Douglas et al., 2015) that affected Mayan city and social structures, caused agricultural abandonment in Costa Rica (Taylor et al., 2020), and disrupted smaller populations in Hispaniola (Lane et al., 2014). There are shifts in available proxy records at ~1000 cal yrs BP documented throughout in the Caribbean, including the Cariaco Basin runoff record (Fig. 9d) linked to ITCZ migration (Fig. 9e). Yet, the hydroclimate response may not be uniform across the Caribbean and thus we wish to contrast the conditions in the northern Caribbean here. Speleothem records from Northwestern Cuba suggest a sharp increase in precipitation at 1000 cal yrs BP (Fensterer et al., 2013) (Fig. 9b) or a more gradual increase throughout the last millennium as indicated by another speleothem (Fensterer et al., 2012). In contrast, there is less rainfall-promoted runoff (Ti) recorded in a lagoon in northwestern Cuba (Gregory et al., 2015) at this time. On Abaco, we find shifts in $\delta^2H_{precip\text{-}corr}$ after 1100 and 900 cal yrs BP (Fig. 9a), which would suggest a contracted NASH and increased rainfall.

It is challenging to resolve the disagreement in the archives from the northern Caribbean at present. As the δ^2H_{28} was modified by mangrove expansion in the last 850 cal yrs BP, and potentially as early as ~1350 cal yrs BP when wetlands first colonized depressions and deposited peat on the adjacent epikarst surface, caution must be used in interpreting δ^2H_{28} from a hydroclimate perspective. At ~700 cal yrs BP, lower $\delta^2H_{precip\text{-}corr}$ values are found to be synchronous with increased pine on the landscape, which perhaps indicates a contracted NASH during the Little Ice Age and broadly wetter climate (Fig. 8). However, even after accounting for the mangrove bias, $\delta^2H_{precip\text{-}corr}$ show ^{2}H-depleted values that may indicate an under-correction of the mangrove influence rather than hydroclimate shifts.

6. Conclusions

Plant wax hydrogen isotopic evidence for past precipitation is modulated by mangrove inputs in a 3000-year sedimentary record from Blackwood Sinkhole, Abaco Island, Bahamas. A prominent increase in mangroves in the last 850 years (van Hengstum et al., 2016; Tamalavage et al., 2018) appears to contribute plant wax *n*-alkyl lipids that are ^{2}H-depleted, consistent with studies on the effects of salinity on hydrogen isotopic fractionation (Ladd et al., 2012). Mangrove presence is readily detected by mangrove specific proxies (pollen, and the mangrove biomarker taraxerol), and changing inputs also modulate the plant wax proxies (plant wax *n*-alkanoic acid and *n*-alkane abundance, as well as $\delta^{13}C_{28}$ and δ^2H_{28}). Using the pollen record, we accounted for the vegetation changes and generated a mangrove-corrected plant wax record that can be interpreted cautiously as a reconstruction of past precipitation isotopes.

Mangrove-corrected precipitation δ^2H reconstructions from Blackwood sinkhole suggest centennial-scale variability in hydroclimate in the Caribbean. Periods of more ^{2}H-enriched values from 2950 to 2100 cal yrs BP and 1700 to 1000 cal yrs BP suggest an expanded NASH and likely more arid conditions over much of the Caribbean. Depletion of ^{2}H from 2100 to 1800 cal yrs BP, and from 850 cal yrs BP to the present may correspond to a contracted NASH, with more local convection and thus wetter conditions on Abaco, consistent with interpretations from another record on Abaco from No Man's Sinkhole. In the last 850 years, pollen assemblages indicate that mangroves compromise the plant wax proxy in Blackwood Sinkhole, modulating the record with ^{2}H-depletion that corresponds to increased mangrove inputs. In this mangrove-influenced interval, the plant wax hydrogen isotopic evidence for precipitation is compromised. Our pollen correction allows for the removal of this bias and suggests a range of precipitation isotopic composition and variability that is consistent with expected atmospheric dynamics and distillation patterns. We suggest that pollen and plant wax provide an invaluable pairing to identify, evaluate, and address mangrove influence on the plant wax hydrogen isotope proxy in similar tropical, coastal sinkhole settings.

Data availability statement

All data associated with this submission are publicly available within the NOAA Paleoclimatology repository: https://www.ncdc.noaa.gov/paleo-search/study/29512.

Declaration of Competing Interest

The authors declare that they have no known competing financial interests or personal relationships that could have appeared to influence the work reported in this paper.

Acknowledgements

Plant wax analyses were funded by US National Science Foundation EAR-1703141 to SF, EAR-1703087 to PvH and by a 2016 Grants-In-Aid of Graduate Research Grant from Texas Sea Grant to AT. Sample collection was supported by OCE-1519578, OCE-1356708 to PvHand JD and BCS-1118340 to PLF. Additional analytical support was funded by EAR-1702946 and AGS-1805480 to SC. This is SOEST publication no. 11137. Field access and permissions were supported by AMMC/National Museum of The Bahamas and permits granted by The Bahamas Environment, Science and Technology (BEST) Commission. Technical field and lab support was provided by L. Lavold-Foote, D. Macdonald, S. Madsen, Y. Wang, R. Sullivan, S. Little, and T. Winkler. Special thanks to R. Sullivan for additional support and analysis. The plant wax analyses were conducted with laboratory assistance at USC from Efrain Vidal and Hyo Sun (Sunny) Lee, with thanks to Nemiah Ladd and Daolai Zhang for helpful guidance. We thank our editor Erdem Idiz and two anonymous reviewers, whose comments improved the manuscript.

Appendix A. Supplementary material

Supplementary data to this article can be found online at https://doi.org/10.1016/j.orggeochem.2020.104120.

Associate Editor—**Kliti Grice**

References

Berman, M.J., Pearsall, D.M., 2000. Plants, people, and culture in the prehistoric central Bahamas: a view from the Three Dog Site, an early Lucayan settlement on San Salvador Island, Bahamas. Latin American Antiquity 11, 219–239.

Bhattacharya, T., Coats, S., 2020. Atlantic-Pacific gradients drive Last Millennium hydroclimate variability in Mesoamerica. Geophysical Research Letters. e2020GL088061.
Bhattacharya, T., Tierney, J.E., DiNezio, P., 2017. Glacial reduction of the North American Monsoon via surface cooling and atmospheric ventilation. Geophysical Research Letters 44, 5113–5122.
Brady, E., Stevenson, S., Bailey, D., Liu, Z., Noone, D., Nusbaumer, J., Otto-Bliesner, B. L., Tabor, C., Tomas, R., Wong, T., 2019. The connected isotopic water cycle in the Community Earth System Model version 1. Journal of Advances in Modeling Earth Systems 11, 2547–2566.
Chikaraishi, Y., Naraoka, H., 2007. δ13C and δD relationships among three n-alkyl compound classes (n-alkanoic acid, n-alkane and n-alkanol) of terrestrial higher plants. Organic Geochemistry 38, 198–215.
Curtis, J.H., Brenner, M., Hodell, D.A., Balser, R.A., Islebe, G.A., Hooghiemstra, H., 1998. A multi-proxy study of Holocene environmental change in the Maya Lowlands of Peten, Guatemala. Journal of Paleolimnology 19, 139–159.
Diefendorf, A.F., Freimuth, E.J., 2017. Extracting the most from terrestrial plant-derived n-alkyl lipids and their carbon isotopes from the sedimentary record: A review. Organic Geochemistry 103, 1–21.
Douglas, P.M., Pagani, M., Brenner, M., Hodell, D.A., Curtis, J.H., 2012. Aridity and vegetation composition are important determinants of leaf-wax δD values in southeastern Mexico and Central America. Geochimica et Cosmochimica Acta 97, 24–45.
Douglas, P.M., Pagani, M., Canuto, M.A., Brenner, M., Hodell, D.A., Eglinton, T.I., Curtis, J.H., 2015. Drought, agricultural adaptation, and sociopolitical collapse in the Maya Lowlands. Proceedings of the National Academy of Sciences 112, 5607–5612.
Ebisuzaki, W., 1997. A method to estimate the statistical significance of a correlation when the data are serially correlated. Journal of Climate 10, 2147–2153.
Feakins, S.J., 2013. Pollen-corrected leaf wax D/H reconstructions of northeast African hydrological changes during the late Miocene. Palaeogeography, Palaeoclimatology, Palaeoecology 374, 62–71.
Feakins, S.J., Bentley, L.P., Salinas, N., Shenkin, A., Blonder, B., Goldsmith, G.R., Ponton, C., Arvin, L.J., Wu, M.S., Peters, T., West, A.J., Martin, R.E., Enquist, B.J., Asner, G.P., Malhi, Y., 2016. Plant leaf wax biomarkers capture gradients in hydrogen isotopes of precipitation from the Andes and Amazon. Geochimica et Cosmochimica Acta 182, 155–172.
Feakins, S.J., Kirby, M.E., Cheetham, M.I., Ibarra, Y., Zimmerman, S.R.H., 2014. Fluctuation in leaf wax D/H ratio from a southern California lake records significant variability in isotopes in precipitation during the late Holocene. Organic Geochemistry 66, 48–59.
Feakins, S.J., Sessions, A.L., 2010a. Controls on the D/H ratios of plant leaf waxes in an arid ecosystem. Geochimica et Cosmochimica Acta 74, 2128–2141.
Feakins, S.J., Sessions, A.L., 2010b. Crassulacean acid metabolism influences D/H ratio of leaf wax in succulent plants. Organic Geochemistry 41, 1269–1276.
Feakins, S.J., Wu, M.S., Ponton, C., Tierney, J.E., 2019. Biomarkers reveal abrupt switches in hydroclimate during the last glacial in southern California. Earth and Planetary Science Letters 515, 164–172.
Fensterer, C., Scholz, D., Hoffmann, D., Spotl, C., Pajon, J.M., Mangini, A., 2012. Cuban stalagmite suggests relationship between Caribbean precipitation and the Atlantic Multidecadal Oscillation during the past 1.3 ka. The Holocene 22, 1405–1412.
Fensterer, C., Scholz, D., Hoffmann, D.L., Spötl, C., Schröder-Ritzrau, A., Horn, C., Pajón, J.M., Mangini, A., 2013. Millennial-scale climate variability during the last 12.5ka recorded in a Caribbean speleothem. Earth and Planetary Science Letters 361, 143–151.
Fornace, K.L., Hughen, K.A., Shanahan, T.M., Fritz, S.C., Baker, P.A., Sylva, S.P., 2014. A 60,000-year record of hydrologic variability in the Central Andes from the hydrogen isotopic composition of leaf waxes in Lake Titicaca sediments. Earth and Planetary Science Letters 408, 263–271.
Fornace, K.L., Whitney, B.S., Galy, V., Hughen, K.A., Mayle, F.E., 2016. Late Quaternary environmental change in the interior South American tropics: new insight from leaf wax stable isotopes. Earth and Planetary Science Letters 438, 75–85.
Freeman, K.H., Pancost, R., 2013. Biomarkers for terrestrial plants and climate. Second Edition. Elsevier Inc., Treatise on Geochemistry, pp. 395–416.
Freimuth, E.J., Diefendorf, A.F., Lowell, T.V., 2017. Hydrogen isotopes of n-alkanes and n-alkanoic acids as tracers of precipitation in a temperate forest and implications for paleorecords. Geochimica et Cosmochimica Acta 206, 166–183.
Fritz, S.C., Björck, S., Rigsby, C.A., Baker, P.A., Calder-Church, A., Conley, D.J., 2011. Caribbean hydrological variability during the Holocene as reconstructed from crater lakes on the island of Grenada. Journal of Quaternary Science 26, 829–838.
Farquhar, G.D., O'Leary, M.H., Berry, J.A., 1982. On the relationship between carbon isotope discrimination and the intercellular carbon dioxide concentration in leaves. Functional Plant Biology 9, 121–137.
Gamble, D.W., Curtis, S., 2008. Caribbean precipitation: review, model and prospect. Progress in Physical Geography 32, 265–276.
Gao, L., Guimond, J., Thomas, E., Huang, Y., 2015. Major trends in leaf wax abundance, δ2H and δ13C values along leaf venation in five species of C3 plants: physiological and geochemical implications. Organic Geochemistry 78, 144–152.
Gregory, B.R.B., Peros, M., Reinhardt, E.G., Donnelly, J.P., 2015. Middle-late Holocene Caribbean aridity inferred from foraminifera and elemental data in sediment cores from two Cuban lagoons. Palaeogeography, Palaeoclimatology, Palaeoecology 426, 229–241.
Hasanean, H., 2004. Variability of the North Atlantic subtropical high and associations with tropical sea-surface temperature. International Journal of Climatology: A Journal of the Royal Meteorological Society 24, 945–957.
Haug, G.H., Günther, D., Peterson, L.C., Sigman, D.M., Hughen, K.A., Aeschlimann, B., 2003. Climate and the collapse of Maya civilization. Science 299, 1731–1735.
Haug, G.H., Hughen, K.A., Sigman, D.M., Peterson, L.C., Rohhl, U., 2001. Southward migration of the intertropical convergence zone through the Holocene. Science 293, 1304–1308.
He, D., Ladd, S.N., Sachs, J.P., Jaffé, R., 2017. Inverse relationship between salinity and 2H/1H fractionation in leaf wax n-alkanes from Florida mangroves. Organic Geochemistry 110, 1–12.
Herrera, D.A., Ault, T.R., Fasullo, J.T., Coats, S.J., Carrillo, C.M., Cook, B.I., Williams, A. P., 2018. Exacerbation of the 2013–2016 Pan-Caribbean drought by anthropogenic warming. Geophysical Research Letters 45, 10,619-610,626.
Hodell, D.A., Brenner, M., Curtis, J.H., 2005. Terminal Classic drought in the northern Maya lowlands inferred from multiple sediment cores in Lake Chichancanab (Mexico). Quaternary Science Reviews 24, 1413–1427.
Hodell, D.A., Curtis, J.H., Jones, G.A., Higuera-Gundy, A., Brenner, M., Binford, M.W., Dorsey, K.T., 1991. Reconstruction of Caribbean climate change over the past 10,500 years. Nature 352, 790.
Horn, S.P., Sanford Jr, R.L., 1992. Holocene fires in Costa Rica. Biotropica, 354–361.
IAEA/WMO, 2019. Global Network of Isotopes in Precipitation. The GNIP Database.
Jury, M., Malmgren, B.A., Winter, A., 2007. Subregional precipitation climate of the Caribbean and relationships with ENSO and NAO. Journal of Geophysical Research: Atmospheres 112.
Kahmen, A., Schefuß, E., Sachse, D., 2013. Leaf water deuterium enrichment shapes leaf wax n-alkane δD values of angiosperm plants I: Experimental evidence and mechanistic insights. Geochimica et Cosmochimica Acta 111, 39–49.
Karnauskas, K.B., Donnelly, J.P., Anchukaitis, K.J., 2016. Future freshwater stress for island populations. Nature Climate Change 6, 720–725.
Karnauskas, K.B., Schleussner, C.-F., Donnelly, J.P., Anchukaitis, K.J., 2018. Freshwater stress on small island developing states: population projections and aridity changes at 1.5 and 2 C. Regional Environmental Change 18, 2273–2282.
Killops, S., Frewin, N., 1994. Triterpenoid diagenesis and cuticular preservation. Organic Geochemistry 21, 1193–1209.
Kjellmark, E., 1996. Late Holocene climate change and human disturbance on Andros Island, Bahamas. Journal of Paleolimnology 15, 133–145.
Koch, B., Rullkötter, J., Lara, R., 2003. Evaluation of triterpenols and sterols as organic matter biomarkers in a mangrove ecosystem in northern Brazil. Wetlands Ecology and Management 11, 257–263.
Ladd, S.N., Sachs, J.P., 2012. Inverse relationship between salinity and n-alkane δD values in the mangrove Avicennia marina. Organic Geochemistry 48, 25–36.
Ladd, S.N., Sachs, J.P., 2013. Positive correlation between salinity and n-alkane δ13C values in the mangrove Avicennia marina. Organic geochemistry 64, 1–8.
Ladd, S.N., Sachs, J.P., 2015a. Hydrogen isotope response to changing salinity and rainfall in Australian mangroves. Plant Cell Environment 38, 2674–2687.
Ladd, S.N., Sachs, J.P., 2015b. Influence of salinity on hydrogen isotope fractionation in Rhizophora mangroves from Micronesia. Geochimica et Cosmochimica Acta 168, 206–221.
Lane, C.S., Horn, S.P., 2013. Terrestrially derived n-alkane δD evidence of shifting Holocene paleohydrology in highland Costa Rica. Arctic, Antarctic, and Alpine Research 45, 342–349.
Lane, C.S., Horn, S.P., Kerr, M.T., 2014. Beyond the Mayan lowlands: impacts of the terminal classic drought in the Caribbean Antilles. Quaternary Science Reviews 86, 89–98.
Lane, C.S., Horn, S.P., Mora, C.I., Orvis, K.H., 2009. Late-Holocene paleoenvironmental change at mid-elevation on the Caribbean slope of the Cordillera Central, Dominican Republic: a multi-site, multi-proxy analysis. Quaternary Science Reviews 28, 2239–2260.
Lane, C.S., Horn, S.P., Taylor, Z.P., Kerr, M.T., 2016. Correlation of bulk sedimentary and compound-specific δ13C values indicates minimal pre-aging of n-alkanes in a small tropical watershed. Quaternary Science Reviews 145, 238–242.
Lee, H., Feakins, S.J., Lu, Z., Schimmelmann, A., Sessions, A.L., Tierney, J.E., Williams, T.J., 2017. Comparison of three methods for the methylation of aliphatic and aromatic compounds. Rapid Communications in Mass Spectrometry 31, 1633–1640.
Lin, G., Sternberg, L.d.S., n and Sternberg 1992. Effect of growth form, salinity, nutrient and sulfide on photosynthesis, carbon isotope discrimination and growth of red mangrove (Rhizophora mangle L.). Functional Plant Biology 19, 509–517.
Lee, J.-E., Johnson, K., Fung, I., 2009. Precipitation over South America during the Last Glacial Maximum: an analysis of the "amount effect" with a water isotope-enabled general circulation model. Geophysical Research Letters 36.
Li, G., Li, L., Tarozo, R., Longo, W.M., Wang, K.J., Dong, H., Huang, Y., 2018. Microbial production of long-chain n-alkanes: implication for interpreting sedimentary leaf wax signals. Organic Geochemistry 115, 24–31.
Li, L., Li, W., Kushnir, Y., 2012. Variation of the North Atlantic subtropical high western ridge and its implication to Southeastern US summer precipitation. Climate Dynamics 39, 1401–1412.
Li, W., Li, L., Fu, R., Deng, Y., Wang, H., 2011. Changes to the North Atlantic subtropical high and its role in the intensification of summer rainfall variability in the southeastern United States. Journal of Climate 24, 1499–1506.
Lin, L., Gettelman, A., Feng, S., Fu, Q., 2015. Simulated climatology and evolution of aridity in the 21st century. Journal of Geophysical Research: Atmospheres 120, 5795–5815.

Liu, W., Yang, H., 2008. Multiple controls for the variability of hydrogen isotopic compositions in higher plant n-alkanes from modern ecosystems. Global Change Biology 14, 2166–2177.
Malaizé, B., Bertran, P., Carbonel, P., Bonnissent, D., Charlier, K., Galop, D., Imbert, D., Serrand, N., Stouvenot, C., Pujol, C., 2011. Hurricanes and climate in the Caribbean during the past 3700 years BP. The Holocene 21, 911–924.
Martin, E.R., Schumacher, C., 2011. Modulation of Caribbean precipitation by the Madden–Julian oscillation. Journal of Climate 24, 813–824.
Martinez, C., Goddard, L., Kushnir, Y., Ting, M., 2019. Seasonal climatology and dynamical mechanisms of rainfall in the Caribbean. Climate Dynamics 53, 825–846.
Nelson, D.B., Sachs, J.P., 2016. Galapagos hydroclimate of the Common Era from paired microalgal and mangrove biomarker 2H/1H values. Proceedings of the National Academy of Sciences of the United States America 113, 3476–3481.
Nelson, D.M., Henderson, A.K., Huang, Y., Hu, F.S., 2013. Influence of terrestrial vegetation on leaf wax δD of Holocene lake sediments. Organic Geochemistry 56, 106–110.
Park, J.W., Ladd, S.N., Sachs, J.P., 2019. Hydrogen and carbon isotope responses to salinity in greenhouse-cultivated mangroves. Organic Geochemistry 132, 23–36.
Sachse, D., Billault, I., Bowen, G.J., Chikaraishi, Y., Dawson, T.E., Feakins, S.J., Freeman, K.H., Magill, C.R., McInerney, F.A., Van Der Meer, M.T., 2012. Molecular paleohydrology: interpreting the hydrogen-isotopic composition of lipid biomarkers from photosynthesizing organisms. Annual Review of Earth and Planetary Sciences 40, 221–249.
Sarkar, S., Prasad, S., Wilkes, H., Riedel, N., Stebich, M., Basavaiah, N., Sachse, D., 2015. Monsoon source shifts during the drying mid-Holocene: biomarker isotope based evidence from the core 'monsoon zone'(CMZ) of India. Quaternary Science Reviews 123, 144–157.
Schefuß, E., Schouten, S., Schneider, R.R., 2005. Climatic controls on central African hydrology during the past 20,000 years. Nature 437, 1003–1006.
Schneider, T., Bischoff, T., Haug, G.H., 2014. Migrations and dynamics of the intertropical convergence zone. Nature 513, 45–53.
Sessions, A.L., Burgoyne, T.W., Schimmelmann, A., Hayes, J.M., 1999. Fractionation of hydrogen isotopes in lipid biosynthesis. Organic Geochemistry 30, 1193–1200.
Slayton, I.A., 2010. A vegetation history from Emerald Pond, Great Abaco Island, the Bahamas, based on pollen analysis.
Smith, F.A., Freeman, K.H., 2006. Influence of physiology and climate on δD of leaf wax n-alkanes from C3 and C4 grasses. Geochimica et Cosmochimica Acta 70, 1172–1187.
Steadman, D.W., Franz, R., Morgan, G., Albury, N.A., Kakuk, B., Broad, K., Franz, S.E., Tinker, K., Pateman, M.P., Lott, T.A., Jarzen, D.M., Dilcher, D.L., 2007. Exceptionally well preserved late Quaternary plant and vertebrate fossils from a blue hole on Abaco, The Bahamas. Proceedings of the National Academy of the Sciences 104, 19897–19902.
Sullivan, R.M., van Hengstum, P.J., Donnelly, J.P., Winkler, T.S., Mark, S.E., Albury, N. A., 2020. Absolute and relative dating of human remains in a Bahamian sinkhole (Great Cistern, Abaco). Journal of Archaeological Science: Reports 32, 102441.
Tamalavage, A.E., van Hengstum, P.J., Louchouarn, P., Molodtsov, S., Kaiser, K., Donnelly, J.P., Albury, N.A., Fall, P.L., 2018. Organic matter sources and lateral sedimentation in a Bahamian karst basin (sinkhole) over the late Holocene: Influence of local vegetation and climate. Palaeogeography, Palaeoclimatology, Palaeoecology 506, 70–83.
Taylor, Z.P., Lane, C.S., Horn, S.P., 2020. A 3600-year record of drought in southern Pacific Costa Rica. Quaternary Research, 1–13.
Tierney, J.E., Russell, J.M., Huang, Y., Damsté, J.S.S., Hopmans, E.C., Cohen, A.S., 2008. Northern hemisphere controls on tropical southeast African climate during the past 60,000 years. Science 322, 252–255.
Tipple, B.J., Berke, M.A., Doman, C.E., Khachaturyan, S., Ehleringer, J.R., 2013. Leaf-wax n-alkanes record the plant–water environment at leaf flush. Proceedings of the National Academy of Sciences 110, 2659–2664.
Urrego, L.E., Bernal, G., Polanía, J., 2009. Comparison of pollen distribution patterns in surface sediments of a Colombian Caribbean mangrove with geomorphology and vegetation. Review of Palaeobotany and Palynology 156, 358–375.
van Hengstum, P.J., Donnelly, J.P., Fall, P.L., Toomey, M.R., Albury, N.A., Kakuk, B., 2016. The intertropical convergence zone modulates intense hurricane strikes on the western North Atlantic margin. Scientific Reports 6, 1–10.
van Hengstum, P.J., Maale, G., Donnelly, J.P., Albury, N.A., Onac, B.P., Sullivan, R.M., Winkler, T.S., Tamalavage, A.E., MacDonald, D., 2018. Drought in the northern Bahamas from 3300 to 2500 years ago. Quaternary Science Reviews 186, 169–185.
Versteegh, G.J., Schefuß, E., Dupont, L., Marret, F., Damsté, J.S.S., Jansen, J.F., 2004. Taraxerol and Rhizophora pollen as proxies for tracking past mangrove ecosystems. Geochimica et Cosmochimica Acta 68, 411–422.
Wu, M.S., Feakins, S.J., Martin, R.E., Shenkin, A., Bentley, L.P., Blonder, B., Salinas, N., Asner, G.P., Malhi, Y., 2017. Altitude effect on leaf wax carbon isotopic composition in humid tropical forests. Geochimica et Cosmochimica Acta 206, 1–17.